JOURNAL OF AGRICULTURAL AND FOOD CHEMISTRY

The Water Vapor Permeability of Polycrystalline Fat Barrier Films

S. MARTINI,† D. A. KIM,‡ M. OLLIVON,§ AND A. G. MARANGONI*,†,§

Department of Food Science, University of Guelph, Guelph, Ontario, Canada, Kraft Foods Global Inc., Glenview, Illinois, and Laboratoire de Physico-Chimie des Systèmes Polyphases, UMR CNRS 8612, Université Paris-Sud, Châtenay-Malabry Cedex, France

The water vapor permeability of fat barrier films has been associated with structural characteristics such as polymorphism, crystal size, and chemical composition, among others. However, no mechanistic models have been proposed to describe this relationship. In this study, we have determined the effects of processing conditions on the structure and physicochemical characteristics of four fats and their relationship to water vapor permeability. Results suggest that the solids' volume fraction and the domain size of the fat crystals seem to be the most important factors controlling water vapor migration. Moreover, materials with relatively large crystalline domains will yield malleable films with relatively low storage and loss moduli and strain/stress at the limit of linearity high tan δ values. The structural effects on the permeability of fat films are related to the nanoscale of the material.

KEYWORDS: Water vapor permeability; water vapor transmission rate; processing conditions; powder X-ray diffractometry; rheology; solid fat content; domain size

INTRODUCTION

Control of moisture content and moisture migration is critical to the quality and safety of many foods. Edible fat films can be used to limit vapor water transfer (*1*). Several studies have shown that some edible films containing hydrophobic substances can limit water vapor transfer (*2*−*4*). Because the principal function of an edible film is to impede moisture transfer, lipids are generally used as the main structural component because of their hydrophobicity.

Significant research has been carried out during the last 20 years on edible moisture barrier films. Some of these studies have compared the permeability of several lipid sources with different degrees of hydrophobicity (*5*−*7*). Also, different film preparation techniques were studied by Martin-Polo et al. (*1*) and Guillard et al. (*8*). Emulsion-based films were also studied (*9*, *10*) together with films formulated solely with triacylglycerols (*11*, *12*). In addition, the effect of lipid components on different polysaccharide-based edible films was studied by Yang and Paulson (*13*).

Although the transmission of oxygen and water vapor through lipid films is usually low, there is a great amount of variability in barrier properties depending on chemical composition and processing conditions used to cast the barrier film. These differences are due to several factors such as solid-state morphological characteristics, including crystal size, shape, and polymorphism (*5*, *12*, *14*). In general, the rate of water transfer increases as the lipid hydrocarbon chain length is decreased and the degree of unsaturation or branching of acyl chains is increased. This occurs because lateral packing of acyl chains is less efficient, causing a reduction in van der Waals' interaction and an increase in hydrocarbon chain mobility. These molecular effects enhance water transport. Although several characteristics of the fat crystal network are associated with low water vapor permeability (WVP), a deeper understanding of the mechanisms involved in this phenomenon is needed. The objective of this work is to study the effect of processing conditions on the structure and physicochemical characteristics of different fat samples and their effect on WVP. A mechanistic model describing the fat film behavior will be proposed according to the results obtained.

MATERIALS AND METHODS

Fat Blends. The four fat blends used in this study were partially hydrogenated palm kernel oil blended with 28% w/w of canola oil (PKO/CO), partially hydrogenated palm kernel oil blended with 27% w/w of canola oil and with the addition of 1% w/w of polyglycerol monostearate as an emulsifier (PKO/CO/E), distilled monoglyceride (Myvacet 7-07k) blended with 27% w/w of canola oil (Myv/CO), and Benefat (BC). Myv/CO and BC are fat blends that form films with good barrier properties. Both PKO/CO and PKO/CO/E blends are two new fat systems whose barrier properties are unknown and need to be studied. These four samples allow the study of a wide range of WVP values, and the relationship with their structural factors can be compared and analyzed between samples. The chemical compositions and melting points of the four fat blends are detailed in **Table 1**. Fat samples were provided by Kraft Foods (Glenview, IL).

* To whom correspondence should be addressed. Tel: (33)1-4683-5623. Fax: (33)1-4683-5312. E-mail: amarango@uoguelph.ca.
† University of Guelph.
‡ Kraft Foods Global Inc..
§ Université Paris-Sud.

10.1021/jf0526341 CCC: $33.50 © 2006 American Chemical Society
Published on Web 02/14/2006

Table 1. Fatty Acid Composition and Melting Points of the Samples Studied

carbon no.	PKO/CO	PKO/CO/E	Myv/CO	BC
6:0	0.22 ± 0.01	0.25 ± 0.01	0	0
8:0	3.42 ± 0.06	3.79 ± 0.19	0	0
10:0	2.90 ± 0.02	3.14 ± 0.13	0	0
12:0	30.80 ± 0.12	32.12 ± 0.73	0	0
14:0	11.64 ± 0.18	11.49 ± 0.29	0.49 ± 0.15	0
16:0	10.55 ± 0.51	9.25 ± 0.80	20.55 ± 1.21	12.67 ± 0.14
18:0	11.78 ± 0.08	9.78 ± 0.29	43.63 ± 1.83	81.16 ± 0.52
18:1	19.00 ± 0.35	20.08 ± 0.26	22.18 ± 0.01	0.45 ± 0.30
18:2	6.48 ± 0.06	6.69 ± 0.25	7.75 ± 0.49	0.71 ± 0.08
18:3 + 20:0	3.21 ± 0.15	3.41 ± 0.28	3.76 ± 0.03	0.52 ± 0.02
total	100	100	100	100
MP (°C)	33.0 ± 0.3	32.2 ± 0.2	37.6 ± 0.1	33.3 ± 0.1

Chemical Composition. The fatty acid composition was determined using gas liquid chromatography. A column of 5 mm outer diameter, 3 mm internal diameter, and 1.5 m in length, packed with 10% silar 9CP on chromosorb W, AW 80/100 mesh, was used in this study. This column was placed in a Shimadzu GC-8A (Kyoto, Japan) gas chromatograph (GC). The chromatograph oven was set at 60 °C, and then, a temperature ramp was programmed from 60 to 210 °C at 8 °C/min. The detector and injector temperatures were set at 230 °C. Nitrogen was used as the carrier gas, and both hydrogen and air were used to feed the flame ionization detection detector. Before chromatographic analysis, methyl esters of the TAG's fatty acids were generated. A 50 mg sample of the fats was placed in a vial and dissolved in 2 mL of isooctane. A 200 μL aliquot of 2 N KOH in MeOH was added to this solution. The mixtures were vortexed for 1 min, and after a 5 min incubation period, two drops of a methyl orange solution were added. Finally, the sample was titrated with 2 N HCl until a pink end point was observed. A 0.5 μL aliquot of the organic phase was injected into the chromatograph. The resulting peaks were integrated using a Shimadzu integrator (C-R3A Chromatopac). Samples Myv/CO and BC contained approximately 50 and 25% of C_2 and C_3 acids, respectively, which are not detected by this GC method. Results reported in **Table 1** for Myv/CO and BC show the fatty acid profile of the longer chain fatty acid fraction (C_4 and longer).

Melting Points. Melting points of the four samples were determined using the capillary AOCS method Cc 1-25.

WVP Experiments. Fat samples were heated to 80 °C for 30 min to ensure complete melting, crystallized under different processing conditions as described below (see crystallization procedure section), and poured on top of a mixture of 37.5% w/w of silica gel (grade 60, 230−400 mesh, Fisher Scientific, NY), 3% w/w of hydroxypropyl methyl cellulose (HPMC E15, The Dow Chemical Co., MI), 13.2% w/w of saturated solution of $MgCl_2 \times 6H_2O$, and 46.3% w/w of deionized water in order to obtain 95% of relative humidity (RH). This ensemble was contained in plastic AQUALAB cups (Decagon Devices, Inc., WA). Samples were stored at 5 °C in sealed desiccators with controlled RH. The RH was fixed to RH = 33% using a saturated solution of $MgCl_2 \times 6H_2O$ (Mallickrodt Baker, Inc., NJ). Samples were weighed at the beginning of the experiment and after different periods of time (1, 2, 6, and 10 weeks), and the weight loss was determined at each period of time. The WVP was determined from this set of experiments. Five replicate experiments for each sample were carried out.

WVP Determination. The WVP was calculated from the water vapor transmission rate (WVTR) values. The WVTR was calculated using the following equation:

$$\mathrm{WVTR} = \mathrm{slope}/A \quad (1)$$

where slope is the slope of a straight line portion of the plot of weight loss vs time (g/days) and A is the area of the film used (cm^2), which for our work was determined to be 12.57 cm^2. Therefore, the units for WVTR are g $days^{-1}$ cm^{-2}. Weight loss was a linear function of time for all samples studied ($0.9 < r^2 < 0.95$). The WVP was calculated as:

$$\mathrm{WVP} = \mathrm{WVTR} \cdot \Delta x/\Delta p \quad (2)$$

where Δx is the thickness of the film (mm) and Δp (mmHg) is the vapor pressure difference between both sides of the film. Therefore, the units for WVP are g mm $days^{-1}$ cm^{-2} $mmHg^{-1}$. The thickness of the film (Δx) was measured at the end of the experiment in the center and the border of the film, and the values were averaged for each sample. Film thickness of the samples varied between 2.10 and 3.10 mm. The pressure gradient (Δp = 4.14 mmHg) was calculated from the water activity value in the desiccator ($a_w = 0.336 \pm 0.0280$) and the filling ($a_w = 0.9693 \pm 0.0183$). The water activity was measured with a water activity meter (AQUALAB, model CX-2, Decagon Devices Inc.) by quintuplicate. The WVP was calculated for each replicate separately and then averaged.

Crystallization Procedure. Four crystallization conditions were used in this work in order to mimic different processing conditions. For all of the different conditions assayed, samples were heated to 80 °C and held at this temperature for 30 min to allow the complete melting of the sample. Afterward, the following crystallization procedures were applied.

(i) Melted samples (80 °C) were poured on top of the silica gel mixture placed in the AQUALAB cups (Decagon Devices, Inc.), cooled to 20 °C at a rate of 10 °C/min, and kept at this temperature for 15 min. Thereafter, samples were transferred to 5 °C storage. This processing condition will be abbreviated as 20-5 °C.

(ii) Melted samples (80 °C) were poured on top of the silica gel mixture, in the AQUALAB cups (Decagon Devices, Inc.), and cooled to 5 °C at a rate of 50 °C/min. This processing condition will be abbreviated as 5 °C.

(iii) Melted samples were cooled from 80 to 20 °C in a beaker at 30 °C/min. After the first crystals were obtained (6−8 min), the sample was poured on top of the silica gel, in the AQUALAB cups (Decagon Devices, Inc.). This processing condition will be abbreviated as 20 °C no shear.

(iv) Melted samples were crystallized as in (iii) but with agitation (200 rpm). This processing condition will be abbreviated as 20 °C shear.

After each crystallization procedure was performed, the cups were placed in a desiccator at a RH of 33% at 5 °C. Samples PKO/CO and PKO/CO/E were crystallized under the four crystallization conditions described above. However, Myv/CO and BC were crystallized using conditions (i) and (ii) only (see explanation in Results section).

Physicochemical Characterization. For all samples crystallized under the different crystallization conditions described above, physicochemical characteristics such as crystal morphology, thermal and rheological behavior, polymorphism, and solid fat content (SFC) were measured as a function of time. Samples were stored using the same procedure as in the WVP experiments (5 °C). At 1, 2, 6, and 10 weeks of storage, the physicochemical characteristics of the samples were also measured.

Crystal Morphology. A small amount of sample, crystallized as described before, was placed between a slide and a coverslip and pressed gently. Polarized micrographs were obtained using a 40× objective lens and a 10× objective lens, respectively, using an Olympus BH microscope (Olympus, Tokyo, Japan). The microscope was equipped with a XC75 CCD camera and LG-3 capture board (Scion Corp., Frederick, United States). Scion Image 1.62 was used to control the camera. Each image represents the average of 16 frames, with the background subtracted. Micrographs were taken for each sample and crystallization condition at different storage times. Pictures were taken in duplicate.

Thermal Behavior. The thermal behavior of the samples was studied by means of a DSC2910 differential scanning calorimeter (DSC) (TA Instruments, Mississauga, Ontario). A 5−10 mg sample of precrystallized fat was placed in an aluminum DSC pan and was heated from crystallization temperature (5 °C) to 80 °C at a rate of 5 °C/min. Each sample and crystallization condition at different storage times was run in duplicate.

Rheology. A TA Instruments AR2000 controlled stress dynamic rheometer (TA Instruments) was used to perform the rheology

Table 2. WVP Values Expressed as g mm days^{-1} cm^{-2} mmHg^{-1} ($\times 10^{-4}$) for All Samples and All Processing Conditions[a]

sample	20-5 °C	5 °C	20 °C shear	20 °C no shear
PKO/CO	4.61 ± 0.61 a	5.35 ± 0.66 a	5.65 ± 1.04 a	3.83 ± 0.47 a
PKO/CO/E	4.03 ± 1.01 a	4.67 ± 0.94 a	4.10 ± 1.14 a	5.43 ± 2.15 a
Myv/CO	2.13 ± 0.20 b	1.50 ± 0.18 b	N/A	N/A
BC	0.44 ± 0.24 b	0.50 ± 0.18 b	N/A	N/A

[a] Values with the same superscript within a column are not significantly different ($P < 0.05$). N/A means not applicable: Myv/CO and BC were not crystallized using the processing conditions detailed in that column.

experiments. Oscillatory tests (small deformation) were performed by means of a strain sweep experiment. The experiments were carried out in a stainless steel parallel plate (20 mm diameter), and the gap was set at 3000 μm for all samples. A constant frequency of 1 Hz was used, and strain values were controlled from 0.003−0.8%. Each sample and crystallization condition at different storage times was run in triplicate.

Powder X-ray Diffraction (XRD). Fat polymorphism was studied with a Multiflex powder X-ray diffractometer (RigakuMSC Inc., The Woodlands, TX). Glass holders with a sample well (0.5 mm depression) were loaded with a sample of crystallized fat. Angular scans was performed at 1°/min from 1 to 30° 2θ using a Cu source X-ray tube at 40 kV and 44 mA. A graphite monochromator was placed between the sample and the detector. Peak detection and analysis were performed using the MDI Jade 6.5 software without baseline subtraction. For the identification of specific polymorphs, the wide angle data for PKO/CO and PKO/CO/E were fitted to a combination of Lorentzian and Gaussian peak forms. This allowed for the removal of the liquid oil-associated scattering and the identification of the reflections associated with specific polymorphs. Fitting of the data to the peak functions was carried out using nonlinear regression (GraphPad Prism 4.0, San Diego, CA). Data were plotted as intensity vs the scattering vector, q, where $q = 2\pi/d$, where d is the interplanar spacing. Each sample and crystallization condition at different storage times was run in duplicate.

Statistical Analysis. The physicochemical parameters studied were correlated to the WVP of the fat films using correlation analysis (GraphPad Prism 4.0).

RESULTS

WVP. The WVP for the four fat blends crystallized under different crystallization conditions is shown in **Table 2**. A one-way analysis of variance (ANOVA) analysis showed that processing conditions did not significantly affect ($P < 0.05$) the WVP of the samples. However, different WVPs were obtained depending on the nature (chemical composition) of the sample. PKO/CO and PKO/CO/E samples had a significantly higher WVP than Myv/CO and BC samples ($P < 0.05$).

Microstructure. Figure 1 shows micrographs of PKO/CO/E sample crystallized under the different crystallization conditions described previously and stored at 5 °C for 10 weeks. We can observe from this figure that when the sample was cooled under 20-5 °C conditions (**Figure 1a**), large crystals were obtained. In fact, this figure shows how they were not single crystals but crystal clusters arranged in a spherulitic-like shape. As expected, when the same sample was cooled under 5 °C conditions (**Figure 1b**), crystals were significantly smaller forming a network of small plateletlike crystals. Surprisingly, when PKO/CO/E was cooled under 20 °C shear or no shear conditions (**Figure 1c**,**d**, respectively), small crystals were obtained resembling the ones obtained when the sample was crystallized

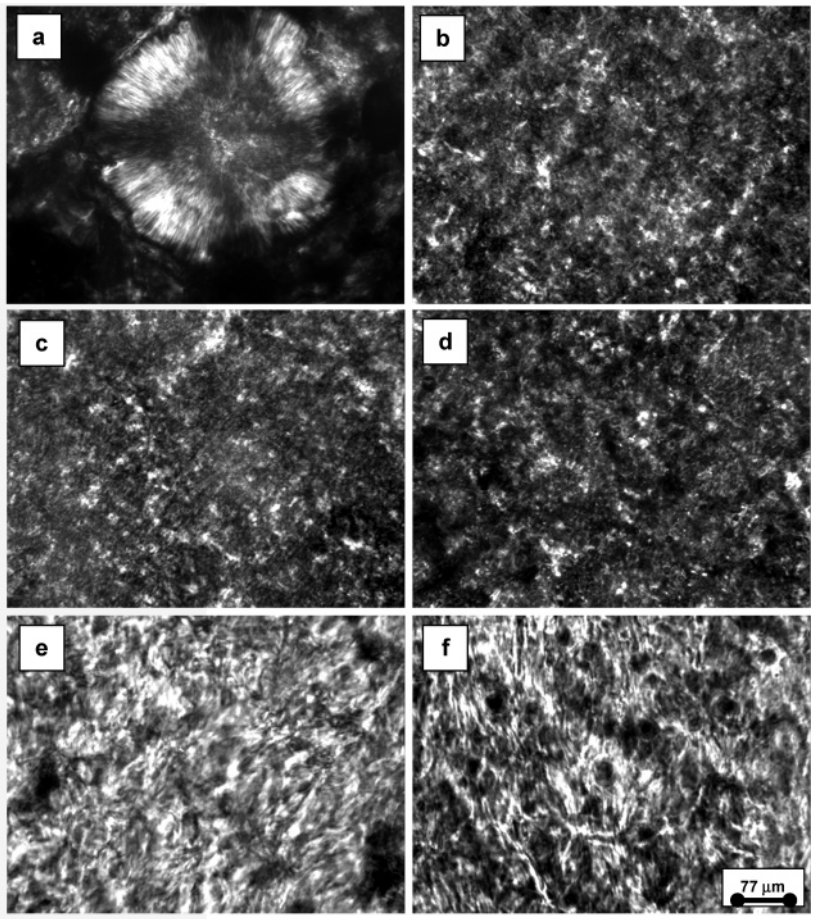

Figure 1. Polarized light micrographs of PKO/CO/E crystallized under different processing conditions: 20-5 °C (**a**), 5 °C (**b**), 20 °C shear (**c**), and 20 °C no shear (**d**). BC sample crystallized at 20-5 °C (**e**) and at 5 °C (**f**). All images were taken after 10 weeks of storage at 5 °C.

Table 3. Variation of Rheological Parameters for Samples Crystallized under Different Processing Conditions[a]

samples	G' ($\times 10^5$, Pa)	G'' ($\times 10^5$, Pa)	tan(δ)	γ^* ($\times 10^{-3}$, %)	σ^* (Pa)
			5 °C		
PKO/CO	13.9 ± 2.0 a	1.58 ± 0.35 a	0.110 ± 0.015 a	3.43 ± 1.20 a	2131 ± 1231 a
PKO/CO/E	38.0 ± 19.3 b	4.92 ± 2.47 a	0.136 ± 0.034 a	2.28 ± 0.77 a	2642 ± 1638 a
Myv/CO	3.35 ± 1.15 a	2.24 ± 0.62 a	0.681 ± 0.066 b	1.36 ± 0.25 b	327 ± 118 b
BC	8.41 ± 4.32 a	4.47 ± 2.69 a	0.540 ± 0.085 c	1.64 ± 0.39 b	1099 ± 993 b
			20-5 °C		
PKO/CO	22.6 ± 9.2 a	3.18 ± 1.50 a	0.134 ± 0.026 a	2.81 ± 0.70 a	2229 ± 721 a
PKO/CO/E	14.5 ± 1.8 b	1.66 ± 0.35 a	0.106 ± 0.014 a	2.38 ± 0.45 a	2233 ± 1218 a
Myv/CO	3.91 ± 1.53 a	2.86 ± 0.95 a	0.733 ± 0.081 b	1.42 ± 0.46 b	501 ± 311 b
BC	3.81 ± 1.48 a	1.64 ± 0.52 a	0.441 ± 0.055 c	1.34 ± 0.31 b	314 ± 76 b
			20 °C no shear		
PKO/CO	17.1 ± 5.0 a	1.81 ± 0.73 a	0.104 ± 0.010 a	3.11 ± 1.25 a	2844 ± 1846 a
PKO/CO/E	21.9 ± 7.3 a	2.54 ± 0.78 a	0.115 ± 0.009 a	2.01 ± 0.38 a	2330 ± 734 a
			20 °C shear		
PKO/CO	15.5 ± 2.5 a	1.83 ± 0.82 a	0.117 ± 0.036 a	2.20 ± 0.90 a	1884 ± 866 a
PKO/CO/E	21.0 ± 8.8 a	2.48 ± 1.41 a	0.111 ± 0.021 a	1.80 ± 0.31 a	2419 ± 884 a

[a] Values with the same letter within a column are not significantly different ($P < 0.05$).

under 5 °C conditions. The same results were obtained for the PKO/CO sample (data not shown). In addition, processing conditions (20-5 and 5 °C) did not affect the microstructure of Myv/CO and BC samples, and in these cases, small crystals were always obtained. **Figure 1e** shows the morphology obtained when the BC sample was crystallized under 20-5 °C conditions and stored for 10 weeks at 5 °C. **Figure 1f** shows the morphology of the same sample but crystallized under 5 °C conditions. The same morphology was observed for the Myv/CO sample (data not shown). Because no differences in morphology were observed for these samples (Myv/CO and BC) when crystallized under such different processing conditions, the next two processing conditions (20 °C shear and no shear) were not studied. The microstructure of the samples was also analyzed during storage at different times, and no significant differences were observed on the morphology of the crystals. Although there was an effect of processing conditions (crystallization temperature and cooling rate) on crystal morphology for PKO/CO and PKO/CO/E samples, no significant differences were found in the WVP as described before and shown in **Table 2**. This suggests that crystal size and morphology at this length scale may not be significant factors influencing the WVP of fat films.

Rheology. Rheological parameters such as storage (G') and loss (G'') moduli, tan δ (tan $\delta = G''/G'$), stress (σ^*), and strain (γ^*) at limit of linearity were measured as a function of storage time for the different samples and processing conditions assayed. No significant differences were found between storage time or processing conditions for all samples and all rheological parameters when a two-way ANOVA was performed ($P < 0.05$). **Table 3** shows the rheology parameters values averaged over time for all samples and all crystallization conditions. A one-way ANOVA analysis was performed to analyze differences between samples. Results show that only the G' values of PKO/CO/E and Myv/CO were significantly different with the latter having lower values. No significant differences were found between G'' values. For tan δ, no significant differences were found between PKO/CO and PKO/CO/E samples, but both Myv/CO and BC had significantly higher values of tan δ ($P < 0.05$). For both γ^* and σ^*, no significant differences ($P > 0.05$) were found between PKO/CO and PKO/CO/E but Myv/CO and BC displayed consistently lower values for these parameters. Myv/CO and BC had lower values of G' and higher tan δ values than PKO/CO and PKO/CO/E. This means that Myv/CO and BC are more malleable since less force is needed to produce a permanent deformation in their structure.

Table 4. Variation of SFC as a Function of Different Crystallization Conditions[a]

	SFC (%)			
samples	5 °C	20-5 °C	20 °C no shear	20 °C shear
PKO/CO	47.20 ± 7.23 a	42.98 ± 7.43 a	39.08 ± 1.94 a	41.82 ± 2.11 a
PKO/CO/E	45.86 ± 5.31 a	35.23 ± 4.55 a	43.10 ± 6.14 a	43.75 ± 7.54 a
Myv/CO	60.86 ± 0.78 b	62.97 ± 0.54 b	N/A	N/A
BC	85.79 ± 1.12 c	85.87 ± 0.40 c	N/A	N/A

[a] Values with the same letter within a column are not significantly different ($P < 0.05$). N/A means not applicable: Myv/CO and BC were not crystallized using the processing conditions detailed in that column.

SFC. SFC was measured during the storage at 5 °C for all samples and all processing conditions. Data were analyzed by means of a two-way ANOVA to study whether the processing conditions and storage time affected the amount of crystallized fat in the sample. Results showed no significant differences between processing conditions or storage time for all samples. **Table 4** shows SFC values obtained as an average over time for all samples and all crystallization conditions. A one-way ANOVA was performed to evaluate whether the SFCs for the different samples were significantly different. The results show that PKO/CO and PKO/CO/E were not significantly different while all of the other samples showed significantly different SFC values: BC had the highest value of SFC, followed by Myv/CO, while the lowest SFC was observed for the PKO/CO and PKO/CO/E samples. **Figure 2A** shows the nonlinear relationship between WVP and SFC values (further discussion below). In this figure, we can observe how low WVP values are associated with high SFCs.

Chemical Composition. Figure 2B shows the relationship between WVP and the percentage of stearic acid of the different samples (**Table 1**). From this figure, we can observe that a high content of stearic acid in the sample is associated with low WVP values, which makes the film less permeable to water vapor.

Thermal Behavior. The thermal behavior of the samples was analyzed by means of a DSC. Both the storage time and the effect of processing conditions were analyzed. A two-way ANOVA analysis was used to determine if there were significant differences in the DSC parameters as a function of time and processing conditions. The DSC parameters analyzed were the

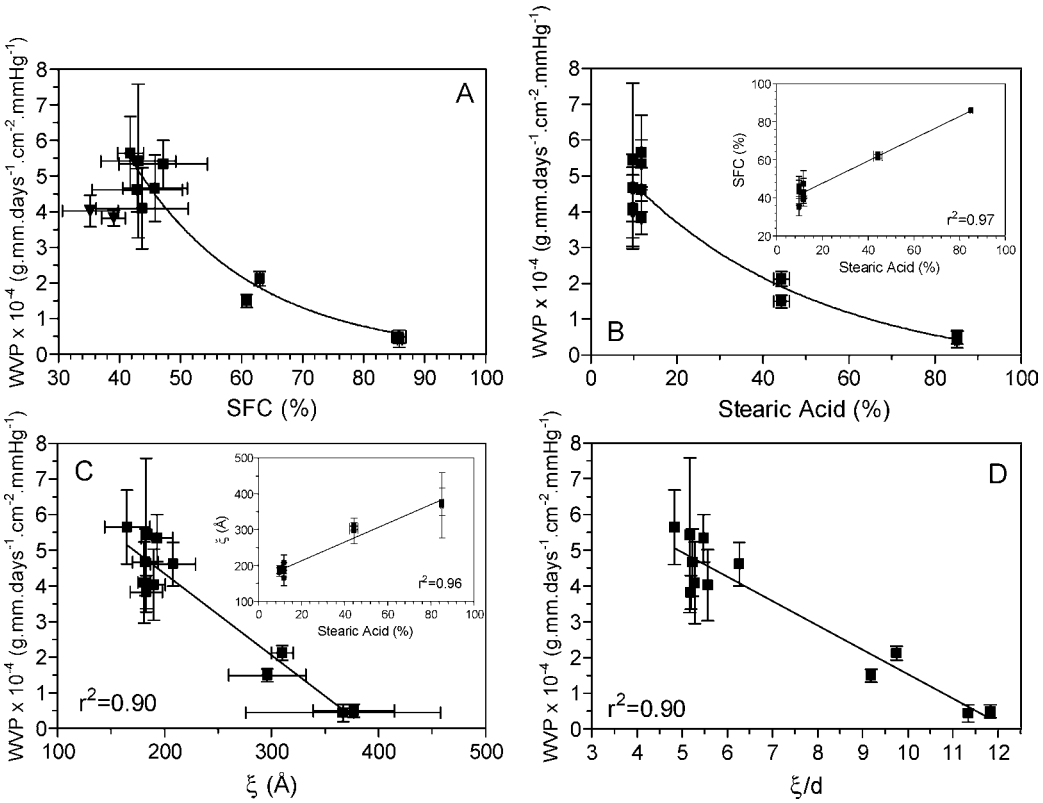

Figure 2. Variation of the WVP with SFC (**A**), the amount of stearic acid (**B**), the crystalline domain size (**C**), and the normalized domain size (**D**) for all samples and processing conditions. The insets depict the correlation between the SFC and the domain size with the stearic acid content.

Table 5. Melting Parameters for Samples Crystallized under All Crystallization Conditions Assayed, Including Onset Temperature (T_o), Peak Temperature (T_p), and Melting Enthalpy (ΔH)[a]

sample	T_o (°C)	T_p (°C)	ΔH (J/g)
	5 °C		
PKO/CO	12.79 ± 1.11 a	23.73 ±0.68 a	70.78 ± 6.10 a
PKO/CO/E	12.47 ± 1.37 a	23.61 ± 0.79 a	70.00 ± 10.50 a
Myv/CO	37.23 ± 0.47 b	42.45 ± 0.75 b	54.70 ± 3.87 a
BC	32.01 ± 0.82 c	35.56 ± 0.36 c	85.49 ± 2.20 b
	20-5 °C		
PKO/CO	13.20 ± 0.48 a	23.36 ± 0.28 a	64.19 ± 6.05 a
PKO/CO/E	12.69 ± 2.24 a	23.52 ± 0.93 a	58.97 ± 14.61 a
Myv/CO	35.92 ± 1.44 b	42.12 ± 0.82 b	54.56 ± 5.45 a
BC	32.69 ± 0.58 c	35.40 ± 0.39 c	88.62 ± 3.54 b
	20 °C no shear		
PKO/CO	12.97 ± 1.22 a	23.85 ± 0.39 a	62.54 ± 12.57 a
PKO/CO/E	12.99 ± 0.82 a	24.10 ± 0.27 a	64.12 ± 6.06 a
	20 °C shear		
PKO/CO	13.68 ± 1.32 a	24.17 ± 0.39 a	63.43 ± 8.26 a
PKO/CO/E	13.49 ± 1.22 a	23.80 ± 0.32 a	59.48 ± 7.94 a

[a] Values with the same letter within a column (processing condition) are not significantly different ($P < 0.05$).

onset temperature (T_o), peak temperature (T_p), and melting enthalpy (ΔH). Results suggested that storage time or processing conditions did not affect significantly the DSC parameters. **Table 5** shows the DSC parameters obtained for each sample and each processing condition and averaged over storage time. We can observe that no significant differences in T_o and T_p values were found between PKO/CO and PKO/CO/E samples. However, these values were significantly different for Myv/CO and BC. Enthalpies of melting were significantly different for the BC sample only.

XRD. Small and wide-angle XRD analysis was used to study the solid-state polymorphism of the triacylglycerol molecules. The values for the interplanar distance (d) and the full width half-maximum (FWHM) of the different reflections were determined in each analysis. Values for the domain size (ξ) were calculated from the FWHM as per a Scherer analysis as $\xi = 2\pi/\Delta q$, where Δq is the FWHM in q space. No significant differences were found in the profile of these patterns when samples were stored during different periods of time and crystallized under different processing conditions. **Figure 3** shows the XRD patterns for PKO/CO (**A**), PKO/CO/E (**B**), Myv/CO (**C**), and BC (**D**) at 20 °C. From the wide-angle region, we can observe a strong broad peak centered at about $2\theta = 20°$ ($d = 4.5$ Å), which arises due to scattering from the liquid phase of samples (oil). The importance of this phase is related to the fat composition, decreasing in intensity from samples **A** to **D** as expected from SFC measurements (**Table 4**). Superimposed on top of this broad peak, the β' crystalline phase is observed as sharp lines at 20.86 and 23.28°, corresponding to a d spacing of 4.24 and 3.81 Å, respectively, for PKO/CO (**A**, inset) and PKO/CO/E (**B**, inset). For Myv/CO (**C**, inset) and BC (**D**, inset), on the other hand, we observe a single reflection at 21.5°, corresponding to a d spacing of 4.13 Å, characteristic of the α phase. In the small-angle region, we can observe that the TAG molecules in the four samples arrange in a typical 2L configuration (**Table 6**). We also noticed that the reflections corresponding to the 001 and 003 planes could be clearly observed in PKO/CO and PKO/CO/E. Interestingly, however, for Myv/CO and BC, the 001, 002, 003, as well as the higher order reflections 004 and 005 could be observed. This suggests a more highly organized crystalline structure, smaller crystal sizes, and/or a more homogeneous crystal size distribution in Myv/CO and BC than in PKO/CO and PKO/CO/E. **Table 6** shows the crystalline interplanar spacings for the 001 reflections and the apparent domain sizes (XS) calculated from the FWHM of the 001 plane reflections. Notice the significantly larger apparent

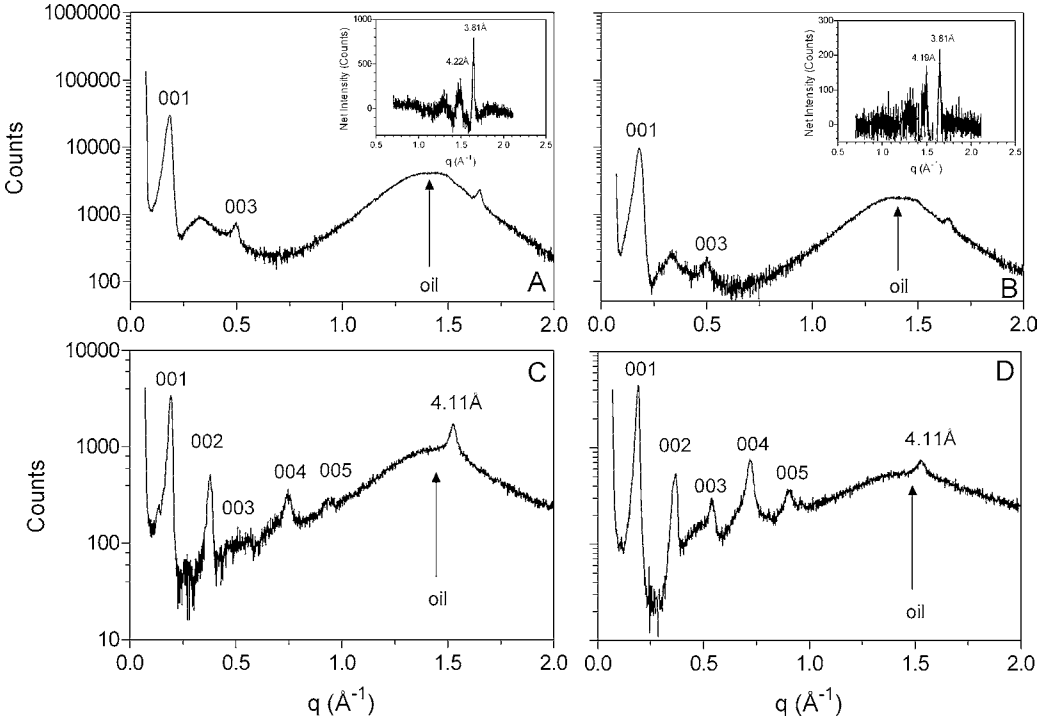

Figure 3. Powder XRD patterns for PKO/CO (**A**), PKO/CO/E (**B**), Myv/CO (**C**), and BC (**D**) crystallized at 20-5 °C and stored at 5 °C for 70 days.

Table 6. Interplanar Spacings (d) and Domain Sizes (ξ) Belonging to Crystals from the Different Fat Barrier Films Crystallized under Different Crystallization Conditions[a]

sample	d_{001} (Å)	ξ_{001} (Å)
	5 °C	
PKO/CO	35.24 ± 0.53 a	193 ± 15 a
PKO/CO/E	34.84 ± 0.97 a	182 ± 12 a
Myv/CO	32.24 ± 0.83 b	296 ± 36 b
BC	31.88 ± 1.78 b	377 ± 38 c
	20-5 °C	
PKO/CO	33.20 ± 1.73 a	208 ± 21 a
PKO/CO/E	34.11 ± 0.98 a	190 ± 11 a
Myv/CO	31.81 ± 1.47 b	310 ± 10 b
BC	32.37 ± 1.24 b	367 ± 91 c
	20 °C without shear	
PKO/CO	35.25 ± 0.58 a	183 ±15 a
PKO/CO/E	35.39 ± 0.43 a	183 ± 5 a
	20 °C with shear	
PKO/CO	34.16 ± 0.83 a	165 ± 21 a
PKO/CO/E	34.25 ± 1.31 a	181 ± 6 a

[a] Values with the same letter within a column (processing condition) are not significantly different ($P < 0.05$).

domain sizes for the Myv/CO and BC samples, indicative of a more ordered crystalline arrangement, smaller crystals, and/or a more homogeneous crystal size distribution.

Figure 2C shows the relationship found between the WVP and the domain size, ξ, for all samples. The same type of relationship was observed when WVP was plotted as a function of ξ/d (**Figure 2D**). Therefore, we could conclude that large ξ values are associated with better moisture barrier properties (low WVP).

Correlations between Structure and WVP. Results discussed previously suggest that there is a general effect of fat rheological properties and thermal behaviors on WVP, but the effect was general in nature. The main result here was that a fat film with a low WVP has to be malleable and have a high solids' content and a high melting point film. Given these

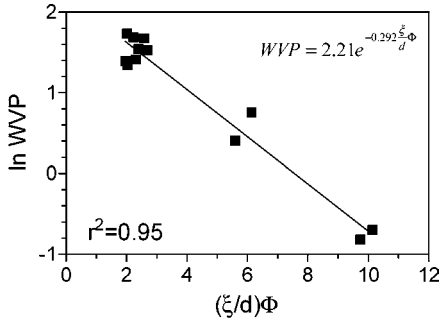

Figure 4. Proposed structural model describing the WVP of laminate fat barrier films.

general conditions, the WVP variation for different samples crystallized under different processing conditions could be described more appropriately using both the SFC and the domain size values (ξ). A low WVP was associated with a high SFC and ξ. This strong correlation suggests a structural component that is responsible for the barrier properties of the material. **Figure 4** shows the proposed model describing the mechanism that governs the migration of water vapor through lipid films. In this figure, we can observe a clear relationship between the WVP and the amount of solids expressed as the volume fraction of solids (Φ = SFC/100) and the ratio of the domain size (ξ) to the lamellar spacing (d). Considering all of the above results, the following equation can be proposed

$$\frac{\mathrm{WVP}}{\mathrm{WVP}_{\max}} = e^{-\alpha(\xi/d)\Phi} \tag{3}$$

$\mathrm{WVP}_{\max}$ is the WVP of the oil in the absence of solids (Φ = 0), and we speculate α to be a parameter related to the tortuosity of the diffusional path through the crystal network. The higher the α value is, the greater the permeability drop as a function of increases in solids' volume fraction. By plotting the ln(WVP) as a function of $(\xi/d)\Phi$, a linear regression can be obtained and α and $\mathrm{WVP}_{\max}$ values can be calculated from the slope and y-intercepts, respectively.

In summary, crystallization conditions used in this study did not seem to affect the WVP of fat barrier films. The apparent domain size (ξ) of the fat crystals, a measure of both the crystalline domain size and the crystalline order in conjunction with the SFC, seem to be the most important factors controlling water vapor migration. It has been previously proposed (*15*) that the movement of permeant molecules through a polymer matrix takes place through the opening of a void space among a series of segments of a polymer chain due to oscillations of the segments, followed by translational motion of the permeant within the void space before the segments return to their "normal state". For the specific conditions and systems assayed in this study, water vapor probably diffuses through the grain boundaries between crystalline domains (*16*). So, if on average the domain size (ξ) is larger, this translates into less grain boundary interfacial area and thus less "holes" through which the water vapor can migrate. This high ξ value necessary for a good water barrier property correlates well with the other physicochemical parameters studied in this work. That is, fats with higher ξ values usually also have a higher SFC. Moreover, the structural characteristics described by a big domain will result in films with lower values of G', higher tan δ, and lower values of γ^* and σ^*. These rheological characteristics are associated with malleable materials. The new model presented in this study proposes a relationship between the water permeability through a fat barrier film and the nanostructure of this material, namely, the crystalline domain size and lamellar spacing.

An interesting point is that a small crystal size was originally believed to be required for low WVP properties, but this was not the case in our study. Both PKO/CO and PKO/CO/E crystallized at 5 °C had small crystals but had a higher WVP than Myv/CO and BC. These findings suggest that the length scale associated with WVP properties of fat films is not the mesoscale but rather the nanoscale of the material.

LITERATURE CITED

(1) Martin Polo, M.; Mauguin, C.; Voilley, A. Hydrophobic films and their efficiency against moisture transfer 1. Influence of the film preparation technique. *J. Agric. Food Chem.* **1992**, *40*, 407−412.

(2) Biquet, B.; Labuza, T. P. Evaluation of the moisture permeability characteristics of chocolate films as an edible moisture barrier *J. Food Sci.* **1988**, *53*, 989−998.

(3) Greener, I. K.; Fennema, O. R. Evaluation of edible bilayer films for use as moisture barrier for food. *J. Food Sci.* **1989**, *54*, 1400−1406.

(4) Guilbert, S.; Biquet, B. In *L'emballage des Denrees Alimentaires de Grande Consummation*; Bureau, G., Multon, J. L., Eds; Lavoisier: Paris, 1989; pp 321−359.

(5) Kester, J. J.; Fennema, O. Resistance of Lipid films to water vapor transmission *J. Am. Oil Chem.* Soc. **1989**, *24*, 1139−1146.

(6) Fennema, O.; Donhowe, I. G.; Kester, J. J. Lipid type and location of the relative humidty gradient influence on the barrier properties of lipids to water vapor. *J. Food Eng.* **1994**, *22*, 225−239.

(7) Bosquez-Molina E.; Guerrero-Legarreta, I.; Vernon-Carter, E. J. Moisture barrier properties and morphology of mesquite gum-candelilla wax based edible emulsion coatings. *Food Res. Int.* **2003**, *36*, 885−893.

(8) Guillard, V.; Guilbert, S.; Bonazzi, C.; Gontard, N. Edible acetylated monoglyceride films: Effect of film-forming technique on moisture barrier properties. *J. Am. Oil Chem. Soc.* **2004**, *81*, 1053−1058.

(9) Quezada Gallo, J. A.; Debeaufort, F.; Callegarin, F.; Voilley, A. Lipid hydrophobicity, physical state and distribution effects on the properties of emulsion-based edible films. *J. Membr. Sci.* **2000**, *180*, 37−46.

(10) Shellhammer, T. H.; Krochta, J. M. Whey protein emulsion film performance as affected by lipid type and amount. *J. Food Sci.* **1997**, *62*, 390−394.

(11) Shellhammer, T. H.; Krochta, J. M. Water vapor barrier and rheological properties of simulated and industrial milkfat fractions. *Trans. ASAE* **1997**, *40*, 1119−1127.

(12) Kester, J. J.; Fennema, O. The influence of polymorphic form on oxygen and water vapor transmission through lipid films. *J. Am. Oil Chem. Soc.* **1989**, *66*, 1147−1153.

(13) Yang, L.; Paulson, A. T. Effects of lipids on mechanical and moisture barrier properties of edible gellan film. *Food Res. Int.* **2000**, *33*, 571−578.

(14) Kester, J. J.; Fennema, O. Resistance of Lipid films to oxygen transmission. *J. Am. Oil Chem. Soc.* **1989**, *24*, 1129−1138.

(15) Miller, K. S.; Krochta, J. M. Oxygen and aroma barrier properties of edible films: A review. *Trends Food Sci. Technol.* **1997**, *8*, 228−237.

(16) Loisel, C.; Lecq, G.; Keller, G.; Ollivon, M. Fat bloom and chocolate structure studied by mercury porosimetry. *J. Food Sci.* **1997**, *62*, 781−788.

Received for review October 24, 2005. Revised manuscript received January 16, 2006. Accepted January 19, 2006. We acknowledge the financial support of the Natural Sciences & Engineering Research Council of Canada (NSERC) and the Ontario Ministry of Agriculture and Food (OMAF). S.M. thanks the National Research Council of Argentina (CONICET) for her postdoctoral fellowship.

JF0526341